JAST, Vol. 5, No. 2, pp 57–66

JAST
Journal of Aerospace Science and Technology

Numerical Simulation of Separation Bubble on Elliptic Cylinders Using Three-Equation $k-\omega$ Turbulence Model

R. Taghavi-Zenouz[1], M. Salari[2], M. Etemadi[3]

Occurrence of laminar separation bubbles on solid walls of an elliptic cylinder has been simulated using a recently developed transitional model for boundary layer flows. Computational method is based on the solution of the Reynolds Averaged Navier-Stokes (RANS) equations and the eddy-viscosity concept. Transitional model tries to simulate streamwise fluctuations, induced by freestream turbulence, in pre-transitional boundary layer flows by introducing an additional transport equation for laminar kinetic energy term. It includes three transport equations of turbulent kinetic energy, K_T, laminar kinetic energy, K_L, and dissipation rate frequency, ω. Numerical results show that the model is capable of predicting each of the subcritical (final separation in laminar), critical (existence of bubble/bubbles) and supercritical (final separation in turbulent) flow regimes. Laminar separation bubble is simulated precisely, due to the modeling of transition from laminar to turbulent in separated free shear layer. Separation bubble region and its characteristics were detected by inspection of the distributions of surface pressure and skin friction, and also through streamlines pattern. Excellent agreements were observed between results obtained through current mathematical modeling and available experimental data for all the flow regimes. In addition, some of the results of the present numerical method are compared to those obtained from application of conventional fully laminar and fully turbulent standard $k-\omega$ models.

NOMENCLATURE

C_μ	Turbulent viscosity coefficient
d	Wall distance (m)
D_T	Near wall Dissipation for turbulent
D_L	Near wall Dissipation for Laminar
f_ν	Viscous damping function
f_{INT}	Intermittency damping function
$f_{\tau,l}$	Time-scale damping function
f_{BP}	Bypass transition parameter
f_{NT}	Natural transition parameter
k	Total fluctuation kinetic energy (k_T+k_L) (m^2/s^2)
P_{k_L}	Laminar kinetic energy production term (m^2/s^3)
P_{k_T}	Turbulent kinetic energy production term (m^2/s^3)
P_ω	Production term governing increase in inverse turbulent time scale $(1/s^2)$
R	Bypass transition production term (m^2/s^3)
R_{NAT}	Natural transition production term (m^2/s^3)
S	Magnitude of mean strain rate tensor, $\sqrt{2S_{ij}S_{ij}}$

1. *Associate Professor, Dept. of Mech. Eng., Iran Univ. of Sci. and Tech., Tehran, Iran, Email: taghavi@iust.ac.ir.*
2. *Phd, Dept. of Mech. Eng., Iran Univ. of Sci. and Tech., Tehran, Iran.*
3. *PhD Candidate, Dept. of Mech. Eng., Iran Univ. of Sci. and Tech., Tehran, Iran.*

S_{ij}	Strain rate tensor, $0.5((\partial U_i/\partial x_j) + (\partial U_j/\partial x_i))$
$-u_i u_j$	Kinematic Reynolds stress tensor (m^2/s^2)
U	x-direction (streamwise) velocity (m/s)
α_T	Turbulent diffusivity for turbulent quantities (m^2/s)
β_{BP}	Bypass transition threshold function
β_{TS}	Tollmien–Schlichting threshold function
β_{NAT}	Natural transition threshold function
ϵ	Farfield turbulent dissipation rate (m^2/s^3)
λ_{eff}	Effective (wall-limited) length scale (m)
λ_T	Turbulent length scale (m)
ν_T	Turbulent kinematic viscosity (m^2/s)
ν_{TOT}	Total (laminar + turbulent) eddy viscosity (m^2/s)
Ω	Magnitude of mean rotation tensor, $\sqrt{2\Omega_{ij}\Omega_{ij}}$
Ω_{ij}	Rotation rate tensor, $0.5((\partial U_i/\partial x_j) - (\partial U_j/\partial x_i))$
ω	Inverse turbulent time scale, ϵ/k_T

INTRODUCTION

External flows past objects have been studied extensively because of their many practical applications. Flow past a blunt body, such as a circular cylinder, usually experiences boundary layer separation and very strong flow oscillations in the wake region behind the body. For these types of flows, boundary layer characteristics (laminar, transitional and turbulent) as well as their separation and consequent wake flow are the main subjects of investigation from both experimental and theoretical point of views.

Flow behind a circular cylinder has become the canonical problem for studying external separated flows. Fluid dynamics of cylinders of elliptical cross-section are also studied due to their wide engineering applications [1]. For example, an effective way to alleviate the undesirable side force resulting from flying at high incidences is changing the conventional cross-section shape from circular to elliptical. This has been a response to the lateral control problems that aircraft with circular cross-section fore-bodies experience at high incidence.

It has been shown that horizontal elliptical fore-bodies exhibit more lateral stability than circular cross-sections or vertical ellipses [2]. Surprisingly, there is very little detailed experimental data for ellipses at Reynolds numbers greater than 100,000. Most experimental and theoretical research works on elliptic bodies are limited to subcritical flow regime, *i.e.*, laminar boundary layer up to final separation points [1]. Flow structure around these bodies depends considerably on the ellipse axes ratio and its incidence angle.

Generally speaking, studying fluid dynamic characteristics of 2-D cylinders set normal to a flow can provide a wide domain of data which can be utilized in 3-D studies. For instance, the forces and moments of inclined bodies can be estimated by using the well-known "cross-flow" theory [3].

Occurrence of separation bubbles on solid walls of bodies immersed in a fluid flow is one of the most striking features in fluid dynamics. The separated flow inside these bubbles could be unstable and could lead to turbulence. The ability to predict and control the dynamic behavior of these separations is of great practical importance. Separation bubbles occur either owing to an adverse pressure gradient or to curvature effects imposed by the geometry of the flow configuration.

In general, there are three distinct flow regimes over the bodies submerged in a fluid flow, which are as follows:

- Subcritical flow - laminar boundary layer up to the final separation point;
- Critical flow - existence of a laminar separation bubble due to laminar separation, followed by transition in the free shear layer region and turbulent re-attachment as well as final turbulent separation;
- Supercritical flow - attached transitional boundary layer followed by final turbulent boundary layer separation [4].

No simplified mathematical treatment is usually possible to determine the real flow field around bodies. It requires solution of the complete Navier-Stokes equations, which depend on the body geometry and flow conditions, and are tedious and time consuming.

Breuer [5] presented 3-D LES simulations of the Circular Cylinder in the subcritical regime ($Re_D = 10^4$-10^5). The finest mesh size was 325×325×64 (325 cells around the circumference of the cylinder). The study implemented several subgrid models to be compared to a benchmark experimental case [6]. The simulations showed separation occuring at 94 degrees, which is downstream of the 'standard' value of 80 degrees.

Selvam [7] performed a series of 2-D LES simulations for $10^4 < Re_D < 10^6$. A finite element approach was used with a 2260 cell mesh. Since no details were given about the flow field, it is difficult to draw conclusions regarding the ability to predict the three distinct flow regimes. RANS-based simulations have shown little success in predicting flow over a blunt body at high Reynolds numbers. This is due to the inability of currently available turbulence models to resolve

the effects of transition. These models are strictly applicable to fully turbulent flow-fields, a condition only approximated for the supercritical regime, and only exactly satisfied as Re?8. Reichel and Strohmeier [8] demonstrated the ability of eddy–viscosity models (SKE, RKE) and LES to predict the drag coefficient for Re_D ranging from 10^2 to 10^7. The grid consisted of 40 cells around the circumference of the cylinder. The study included a band of collected experimental data from the literature, and concluded that predicted values fall within a very close range of the band to justify the use of fully turbulent models. It is difficult to judge the validity of the predictions without an examination of transition, separation, *etc.* in each flow regime.

Catalano *et.al.* [9] compared 2-D results for LES and SKE using wall functions at critical and supercritical Reynolds numbers. The authors also found little sensitivity of the drag coefficient to Re_D in the critical regime, and were unable to capture the separation bubble observed experimentally in this case.

A typical method for including transitional effects is to artificially trip turbulence. Celik and Shaffer [10] used SKE and 2-D steady simulations to study flows (10^4<Re_D<10^7) on a mesh of 100×150 cells. The study implemented an empirical a priori method of fixing the transition point. For Re_D =3.6×10^6, the results showed that the flow separated at 118 degrees. Travin *et.al.* [11] applied the detached eddy simulation technique to the 3-D cylinder in cross flow. For Re_D =5×10^4, a laminar separation was forced. For Re_D =1.4×10^5 and 3×10^6, a turbulent separation was forced. The artificial nature of the transition and the inability to obtain a grid-independent solution were two shortcomings of the work.

Saghaffan *et.al.* [12] performed a series of 2-D unsteady simulations of flow past a circular cylinder for Reynolds numbers ranging from 2×10^3 to 8.4×10^6. The mesh consisted of 16800 cells. The authors employed both linear and non-linear eddy–viscosity models. Results from the linear model showed no transition. When the non-linear, cubic eddy–viscosity model of Craft *et.al.* [13] was employed, a transition was captured. However, the model was unable to predict the separation bubble present in the critical flow.

Edwards *et.al.* [14] performed a series of 2-D unsteady simulations of flow past a heated cylinder for Reynolds numbers ranging from 1.27×10^6 to 4×10^6. The geometry consisted of a half cylinder with centerline symmetry, and the mesh consisted of up to 100000 cells. The authors developed a 1-equation transition model based on the Spalart–Allmaras turbulence model [15] and the work of Warren and Hassan [16,17]. Since all of the test cases were for supercritical flow, transition occurred on the surface of the cylinder. Prediction of the point of transition was good; however, heat transfer was over-predicted. Critical and subcritical test cases were not considered due to their inability to predict separation-induced transition.

In this work, a three equation eddy-viscosity turbulence model has been implemented in an in-house code developed for solving governing equations of two-dimensional viscous flows. The potential of this turbulence model in prediction of transitional flows, enabled the present computational modeling to predict every laminar, transitional or turbulent flow regime. Another advantage of the above turbulence model was its ability to predict occurrence of separation bubble, depending on the freestream Reynolds number and model incidence [4].

CONCEPTS AND FORMULATION

The pre-transitional region of a boundary layer subjected to freestream turbulence (Tu) resembles a laminar boundary layer. As Tu increases, the time-averaged velocity profile becomes noticeably distorted from the Blasius's boundary layer solution. This distortion is due to an increase in the momentum of particles in the inner region in comparison to the outer region of the boundary layer, even for Tu values lower than about 1%[18]. This change of mean velocity profile is accompanied by development of relatively high-amplitude streamwise fluctuations, which can exceed several times that of the free-stream [19]. Subsequently, it leads to occurrence of transition phenomenon through the eventual breakdown of these streamwise fluctuations. This process is accompanied by an increase in skin friction and heat transfer rate. It is important to note that these streamwise fluctuations within the pre-transitional region are not turbulence. The distinction was first introduced by Mayle and Schulz [20] for mathematical modeling purposes. They proposed a laminar-kinetic-energy transport equation to describe the development of such fluctuations. Structurally, these fluctuations are very different from those in turbulent boundary layers, because the energy is almost entirely contained in the streamwise component. Even in fully turbulent flow, there is still evidence of laminar fluctuations very near the solid wall, although their magnitudes are relatively small. This is likely due to the similarity between the viscous sublayer of the turbulent boundary layer and the pre-transitional boundary layer with high free stream turbulence. The considerations have led them to introduce a new kinetic energy equation for description of such fluctuations. Mayle and Schulz designated this energy term as K_L. This transport equation is added to other transport equations for their proposed model, namely, the turbulent kinetic energy K_T and the far-field dissipation ϵ.

Volino [21] considered the possibility that growth

of K_L is due to a splat mechanism, similar to that discussed by Bradshaw [22]. Wall redirects the normal fluctuation into a streamwise component while creating local pressure gradients in the boundary layer leading to disturbance amplification. Based on this mechanism, it is assumed in this model that the turbulent energy spectrum can be divided into wall-limited (large scales) and non-wall-limited (small scales) sections in the near-wall region. The small and large scale components of K_T are designated by $K_{T,s}$ and $K_{T,l}$, respectively. Note that far from the solid wall, *i.e.*, in the free shear layer, $K_{T,s}$ approaches K_T, and $K_{T,l}$ equals zero due to the absence of the splat mechanism. These observations suggest that a relatively simple modeling approach may be capable of resolving the fluctuation growth in the pre-transitional region.

Another region of interest is the transition zone itself. Jacobs and Durbin [23] showed that boundary layer transition in high disturbance environments, called bypass transition, is initiated by instability of the upstream fluctuations. Downstream of transition, almost all of the fluctuation energy is turbulent, but a small amount of K_L is still present within the viscous sub-layer.

The original model of Walters & Laylek [24] uses the turbulence far field dissipation rate, ϵ. However, Holloway *et.al.* [4] used dissipation rate frequency, ω, instead of ϵ, based on the belief that the former parameter leads to a better representation of the breakdown of the laminar kinetic energy to the turbulence kinetic energy.

Consequently, all the above considerations led to the use of formulations presented by Holloway *et.al.* [4], in their studies. The model includes three transport equations introduced as the laminar kinetic energy, K_L, the turbulent kinetic energy, K_T, and dissipation rate frequency, shown by ω, as follows:

$$\frac{Dk_T}{Dt} = \frac{\partial}{\partial x_j}.\left(\nu + \frac{\alpha_T}{\sigma_k}\right)\frac{\partial k_T}{\partial x_j} + P_{k_T} + R + R_{NAT} - \epsilon - D_T \tag{1}$$

$$\frac{Dk_L}{Dt} = \frac{\partial}{\partial x_j}\left[\nu\frac{\partial k_L}{\partial x_j}\right]. + P_{k_L} - R - R_{NAT} - D_L \tag{2}$$

$$\frac{D\omega}{Dt} = \frac{\partial}{\partial x_j}\left(\nu + \frac{\alpha_T}{\sigma_\epsilon}\right)\frac{\partial \epsilon}{\partial x_j} + C_{\omega R}\frac{\omega}{k_L}(R + R_{NAT}) - C_{\omega 2}\omega + C_{\omega 3} f_\omega \alpha_T \left(\frac{\lambda_{eff}}{\lambda_T}\right)^{\frac{4}{3}} \frac{\sqrt{k_T}}{d^3} + P_\omega \tag{3}$$

In this model, prediction of the onset of transition is based on a local parameter, which depends on the turbulent energy and effective length scale. Once this parameter reaches a certain value, transition is assumed to begin and energy from the streamwise fluctuations (K_L) transfers to the turbulent fluctuations (K_T). Threshold values are separately defined for predicting both the natural and bypass transition mechanisms.

The influence of turbulent and laminar fluctuations on the mean flow is included through prescription of a total eddy viscosity (ν_{TOT}) introduced as:

$$-\overline{u_i u_j} = \nu_{_{TOT}}\left(\frac{\partial U_i}{\partial x_j} + \frac{\partial U_j}{\partial x_i}\right) - \frac{2}{3}k_{_{TOT}}\delta_{ij} \tag{4}$$

The effective length scale (λ_{eff}) and turbulence length scale (λ_T) are defined as:

$$\lambda_{eff} = \min\left(C_\lambda\, d, \lambda_T\right) \tag{5}$$

and:

$$\lambda_T = \frac{k^{1.5}}{\epsilon} \tag{6}$$

respectively. Where, d is the distance to the closest solid wall and C_λ is a constant number. Small and large scale energies (designated by $K_{T,s}$ and $K_{T,l}$, respectively) are then calculated assuming the Kolmogorov inertial range spectrum applied over all wave numbers greater than $1/\lambda_T$ [24]. These parameters are introduced as:

$$k_{T,s} = k_T\left(\frac{\lambda_{eff}}{\lambda_T}\right)^{\frac{2}{3}} \tag{7}$$

and:

$$k_{T,l} = k_T\left[1 - \left(\frac{\lambda_{eff}}{\lambda_T}\right)^{\frac{2}{3}}\right] \tag{8}$$

The summation of these two equations forms the turbulent kinetic energy, *i.e.*, K_T.

The production of turbulence by turbulent fluctuations is prescribed, versus the mean strain rate, as $P_{k_T} = \nu_{_{T,s}} S^2$. The small-scale turbulent viscosity, $\nu_{_{T,s}}$, is defined as:

$$\nu_{T,s} = \min\left(f_\nu f_{_{INT}} C_\mu \sqrt{k_{T,s}}\,\lambda_{eff}, \frac{2.5\,\epsilon_{_{TOT}}}{S^2}\right) \tag{9}$$

in which C_μ is a constant number. The above limit on turbulent viscosity is imposed to prevent too rapid production in cases of boundary layer separation as well as in highly strained freestream regions. Other terms appearing in the definition of turbulent viscosity are obtained as follows:

$$C_\mu = \frac{1}{A_0 + A_s\left(\frac{S}{k_T\epsilon}\right)} \tag{10}$$

$$f_\nu = 1 - \exp\left(-\frac{\sqrt{\mathrm{Re}_{T,s}}}{A_\nu}\right),$$

$$\mathrm{Re}_{T,s} = \frac{k_{T,s}^2}{\nu\,\epsilon} \tag{11}$$

$$f_{INT} = \min\left(\frac{k_L}{C_{INT}k_{TOT}}, 1\right) \tag{12}$$

where, A_0, A_s and A_υ are constant numbers. f_{INT} defines a damping function for turbulent production due to intermittency, and is a modification to the original model introduced by Walters and Laylek [24]. This term helps to prevent over-prediction of momentum and scalar transport in the later stages of bypass transition.

The production of laminar kinetic energy by large-scale turbulent fluctuations is introduced as $P_{k_L} = \nu_{T,l} S^2$. The large-scale turbulent viscosity $\nu_{T,l}$ is presented as:

$$\nu_{T,l} = \min\left(\nu_{T,l}^*, \frac{0.5\,k_{T,l}}{S}\right) \tag{13}$$

with

$$\nu_{T,l}^* = f_{T,l} C_{l1} \left(\frac{\Omega \lambda_{eff}^2}{\nu}\right) \sqrt{k_{T,l}}\,\lambda_{eff} + \beta_{TS}\, C_{l2}\, \phi_{NAT}\, d^2\Omega \tag{14}$$

C_{l1} is a constant number. The limit introduced in $\nu_{T,l}$ ensures that realizability is not violated in developing pre-transitional boundary layer. The time-scale-based damping function $f_{T,l}$ is introduced as:

$$f_{\tau,l} = 1 - \exp\left[-C_{\tau,l}\left(\frac{\tau_m}{\tau_{T,l}}\right)^2\right] \tag{15}$$

in which $C_{\tau,l}$ is a constant, and:

$$\tau_{T,l} = \frac{\lambda_{eff}}{\sqrt{k_{T,l}}} \tag{16}$$

and:

$$\tau_m = \frac{1}{\Omega} \tag{17}$$

β_{TS}, ϕ_{NAT} appeared in equation already presented for $\nu_{T,l}^*$, which can be written as:

$$\beta_{TS} = 1 - \exp\left(-\frac{\max\left(\phi_{NAT} - C_{TS,crit}, 0\right)^2}{A_{TS}}\right) \tag{18}$$

where $C_{TS,crit}$ is a constant and:

$$\phi_{NAT} = \frac{d^2\Omega}{\nu} \tag{19}$$

respectively. Near-wall dissipation for turbulent (D_T) and laminar (D_L) regions are given by:

$$D_T = 2\nu \frac{\partial\sqrt{k_T}}{\partial x_j}\frac{\partial\sqrt{k_T}}{\partial x_j} \tag{20}$$

and:

$$D_L = 2\nu \frac{\partial\sqrt{k_L}}{\partial x_j}\frac{\partial\sqrt{k_L}}{\partial x_j} \tag{21}$$

The total dissipation rate of fluctuation energy, ϵ_{TOT}, is defined as:

$$\epsilon_{TOT} = \epsilon + D_L + D_T \tag{22}$$

The term R, which has appeared in transport equations, represents the average effect of the breakdown of streamwise fluctuations into turbulence during bypass transition. It is introduced by Walters and Laylek [24] as follows:

$$R = C_R\,\beta_{BP}\,k_L\,\omega\left(\frac{\lambda_T}{\lambda_{eff}}\right)^{\frac{2}{3}} \tag{23}$$

The threshold function β_{BP} controls the bypass transition process and C_R is a constant. It can be written as:

$$\beta_{BP} = 1 - \exp\left(-\frac{\phi_{BP}}{A_{BP}}\right) \tag{24}$$

with

$$\phi_{BP} = \max\left[\left(\frac{\sqrt{k_T}d}{\nu} - C_{BP,crit}\right), 0\right] \tag{25}$$

In which $C_{BP,crit}$ is a constant number. The breakdown to turbulence due to instabilities is included as a separate natural transition production term as:

$$R_{NAT} = C_{R,NAT}\,\beta_{NAT}\,k_L\,\Omega \tag{26}$$

$C_{R,NAT}$ is a constant and:

$$\beta_{NAT} = 1 - \exp\left(-\frac{\max\left(\phi_{NAT}^{0.75}\phi_{MIX}^{0.25} - C_{NAT,crit}, 0\right)}{A_{NAT}}\right) \tag{27}$$

and

$$\phi_{MIX} = \frac{\sqrt{k_L}d}{\nu} \tag{28}$$

The coefficient $C_{\omega R}$, in transport equation for ω, enforces a reduction of turbulent length scale during the transition breakdown, and takes the functional form of:

$$C_{\omega R} = 1.5\left(\frac{\lambda_T}{\lambda_{eff}}\right)^{\frac{2}{3}} - 1 \tag{29}$$

P_ω, which has appeared in the transport equation, indicates the dissipation rate frequency due to either turbulence production mechanisms or flow field instabilities. It is introduced as:

$$P_\omega = \left(C_{\omega l}\nu_{T,\omega}S^2 + f_{\Delta P}C_{\Delta P}k_{T,l}\Omega\right)\frac{\omega}{k_T} \tag{30}$$

The first term inside the parenthesis is due to turbulent production, where the effective turbulent viscosity corresponds to $\nu_{T,s}$ without any imposed limit. This term can be written as:

$$\nu_{T,\omega} = f_\nu f_{INT} C_\mu \sqrt{k_{T,s}}\lambda_{eff} \tag{31}$$

The second term inside the parenthesis represents the increase in dissipation rate frequency in unstable regions of the boundary layer subjected to an adverse pressure gradient. The damping function $f_{\Delta P}$ is a function of the gradient of the magnitude of the rotation rate tensor in the wall-normal direction, and takes the following forms:

$$f_{\Delta P} = f_{\tau,l} \text{ if } \frac{\partial\Omega}{\partial d} > 0$$
$$f_{\Delta P} = 0 \text{ if } \frac{\partial\Omega}{\partial d} \leq 0 \tag{32}$$

The coefficient $C_{\omega 2}$ is given in the following form:

$$C_{\omega 2} = 0.92\left(\frac{\lambda_{eff}}{\lambda_T}\right)^{\frac{4}{3}} \tag{33}$$

This form enforces a decrease in the turbulent length scale close to the wall.

The use of ω as the scale-determining variable can lead to a reduced intermittency effect in the outer region of a turbulent boundary layer, and consequently an elimination of the wake region in the velocity profile. So the fourth term on the right hand side of ω transport equation is included to rectify this. This term includes the following damping function:

$$f_\omega = 1 - \exp\left[-0.41\left(\frac{\lambda_{eff}}{\lambda_T}\right)^4\right] \tag{34}$$

The total eddy-viscosity is given by:

$$\nu_{TOT} = \nu_{T,s} + \nu_{T,l} \tag{35}$$

Finally, the turbulent scalar diffusivity in ω and K_T transport equations, *i.e.*, α_T is given by:

$$\alpha_T = f_\nu C_{\mu,std}\sqrt{k_T}\lambda_{eff} \tag{36}$$

$C_{\mu,std}$ is a constant. The inlet boundary conditions for K_T and ω are set as those suitable for any two-equation models to reproduce the desired turbulence intensity and length scale. Far from any solid boundary, K_L is set to zero, since the inlet boundary condition is located in the freestream. On the solid walls, all three equations of the computational model of interest use zero-flux boundary conditions; *i.e.*,

$$\frac{\partial k_T}{\partial\eta} = 0, \quad \frac{\partial k_L}{\partial\eta} = 0, \quad \frac{\partial\omega}{\partial\eta} = 0 \tag{37}$$

To evaluate the gradient terms on the wall in D_T and D_L equations, the wall values of $\sqrt{k_T}$ and $\sqrt{k_L}$ are considered equal to zero. This choice of boundary condition eliminates any diffusive transport of fluctuation energy out of the domain. It also leads to very small finite values of k_T and k_L being computed at the wall in the simulations. These wall values do not directly influence the simulation and can be set to zero during post-processing without detriment. During the simulation, the wall values of k_T and k_L used to compute the gradients in Eqs. 20 and 21 are set to zero [24]. This is performed independently of the boundary condition for K_T and K_L. The above model equations and boundary conditions yield the correct asymptotic behavior at solid boundaries, *i.e.* $k \backsim d^2$ and $\epsilon_{TOT} \to 2\nu\, k/d^2$ as $d \to 0$. The constants encountered in the computational model of interest are adequately introduced by Holloway *et.al.* [4].

TEST MODEL AND COMPUTATIONAL IMPLEMENTATION

The model is a two dimensional elliptic cylinder of minor to major axes ratio of 0.6. In the present research work, flow field around this model is investigated only at zero incidences (*i.e.*, the major axis along the main flow direction). Different Reynolds numbers were investigated to establish all the three flow regimes already introduced in this paper.

The mesh structure generated around the model consisted of multi-topology and multi-block grid for all regimes as is shown in Figure 1. Grid independency study was carried out, and in addition, Y^+ values were checked, precisely, for the purposes of the mathematical calculations. Results of Y^+ variations along the model surface are shown in Figure 2.

The equations of the computational model have been implemented in an in-house code, which uses the general non-orthogonal, segregated finite volume scheme. Convection of all transported properties was approximated by the second-order upwind scheme. Mass conservation was enforced via the SIMPLE pressure-correction algorithm, which yields the correct pressure field by an iterative sequence and essentially nullifies the mass residuals in all computational cells.

RESULTS AND DISCUSSIONS

Three distinct cases of subcritical, critical and supercritical flow regimes are studied in the present

work. Experimental results of Taghavi [25] have been used for the selection of the corresponding Reynolds numbers consistent with the above flow regimes. He has tested 2-D and 3-D elliptic bodies of the same cross-sectional thickness ratio of 0.6 at different incidences and Reynolds numbers in a large closed circuit wind tunnel. For the first case, *i.e.*, subcritical case, a Reynolds number of 100000 is selected for the present computational purposes. Reynolds numbers of 600000 and 1040000 are also selected for the critical and supercritical cases, respectively.

The results are presented in terms of surface distributions of pressure and skin friction coefficient for three distinct flow regimes of subcritical, critical and supercritical. Occurrence of transition is generally identified by inspection of skin friction coefficient variation along the surface. The skin friction coefficient is a very sensitive indicator of transition, which increases dramatically as it occurs. Numerical results obtained through application of conventional fully laminar and fully turbulent standard $k-\omega$ models are also superimposed in some of the final results for reference and comparison purposes.

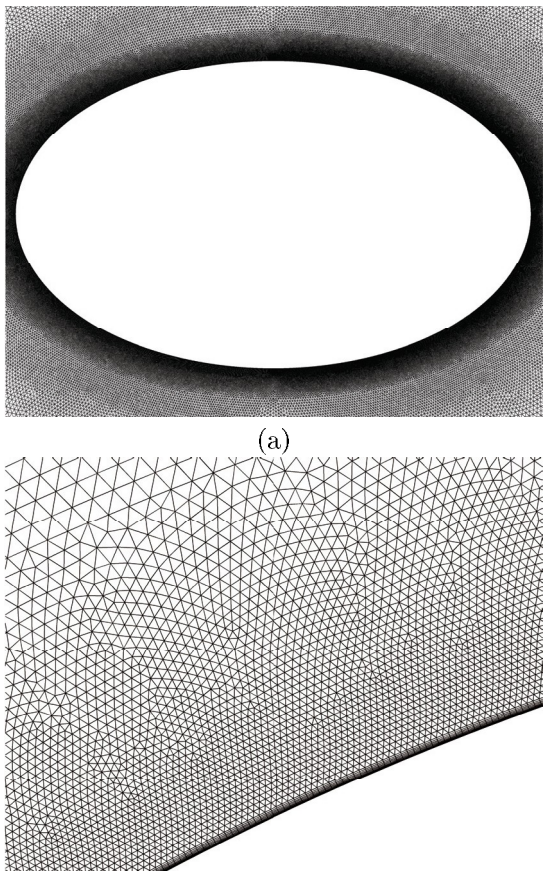

(a)

(b)

Figure 1. Mesh structure close to the model surface.

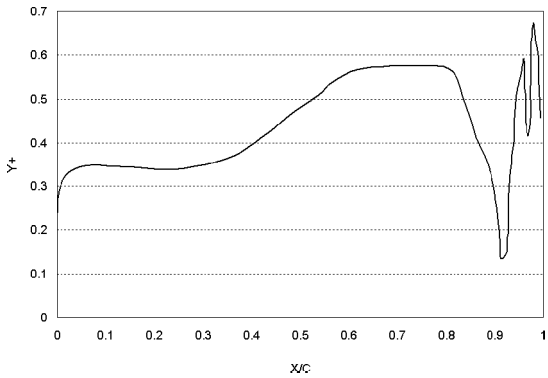

Figure 2. Variations of Y^+ along the model surface.

a) Critical flow

As has already been mentioned, based on the available experimental results of Taghavi [25], separation bubbles can occur on either side of the ellipse at a Reynolds number of 600000. Obviously, flow past this blunt body experiences leeward vortex shedding of a particular frequency consistent with the above freestream Reynolds number. Flow pattern around the ellipse at a specified time is shown in Figure 3. The area in which a separation bubble has been formed aft of the maximum thickness is highlighted and shown in more detail. In addition, the structure of instantaneous leeward vortices can be observed clearly.

Figures 4a and b show surface pressure and skin friction results for this critical case, respectively. In these figures, the horizontal axis shows the normalized arc length with respect to the ellipse semi-perimeter. At this Reynolds number, transition from laminar to turbulent has occurred within the free shear layer. Then, since the turbulent flow is more energetic than the laminar flow it has re-attached to the surface and consequently has formed a bubble on the surface. Generally speaking, a separation bubble consists of an initial region of constant pressure (so-called, stationary part) and a second region in which the pressure rises suddenly (so-called, circulatory region). This clarification leads to the distinction of the position of separation bubble formed on the surface. As has already been mentioned, this is referred to as critical flow regime.

As can be understood from Figure 4a, current numerical approach shows how the present numerical approach has been able to model transition from laminar to turbulent within the free shear layer and the consequent re-attachment of the turbulent flow. Comparison of the present numerical results with the experimental data renders very close agreement. This proves the high capability of the current numerical method in modeling such a complicated flow regime. Neither fully laminar nor fully turbulent modeling has been able to follow the results obtained from the present computational model.

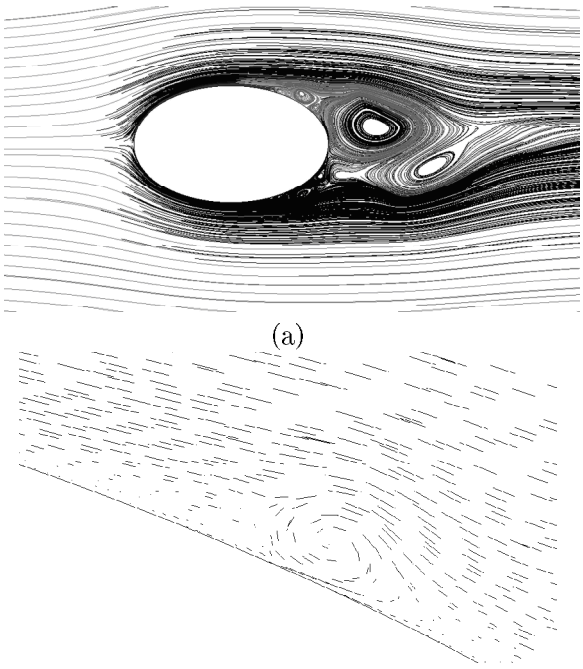

(a)

(b) Velocity vectors within the bubble and its surrounding.

Figure 3. Flow pattern around the ellipse at a specified time, Re=600000.

Generally speaking, a laminar separation bubble is accompanied by zero skin frictions at both the laminar separation (*i.e.*, the beginning point of bubble) and turbulent re-attachment (*i.e.*, the end point of bubble) points. The area of negative local skin friction coefficient, in Figure 4b, reveals a laminar separation bubble on either side of the ellipse aft of the maximum thickness. Approximate position of transition onset point in the free shear layer above the bubble can be recognized by the position where the skin friction starts to grow dramatically from its minimum value. This point is designated by letter T in Figure 4b and also in Figure 3a for the pressure results. Since the re-attached turbulent flow is more energetic than the laminar one, it has resisted the adverse pressure gradient up to the normalized position of %88, where it has separated from the surface (see Figures 4a and b). It is obvious from Figure 4a that the k-w model has failed to predict the occurrence of laminar separation bubble/bubbles.

b) Subcritical and supercritical flows

As has already been mentioned, based on available experimental results of Taghavi [25], subcritical and supercritical cases can occur at the Reynolds numbers of 100000 and 1040000, respectively. Surface pressure and skin friction results for the subcritical flow regime are shown in Figures 5a and b, and for the supercritical case in Figures 6a and b.

Wide wake region, accompanied by nearly a constant suction region, can be clearly identified in Figure 5a, presented for subcritical case. Fully laminar modeling well agrees with the present results up to the position of the maximum thickness, then, it deviates from them within the wake region. Fully turbulent modeling, using standard $k-\omega$ turbulence model, has produced results obviously very far from the present numerical results.

Figure 5b shows the skin friction results for the subcritical case at a Reynolds number of 100000. Velocity gradient at the normal direction to the surface is zero at the point of boundary layer separation, which in turn, causes zero skin friction at this point. Large region of negative skin friction aft of the maximum thickness indicates wide wake due to the boundary layer separation on either side of the ellipse. This is consistent with the pressure results already discussed for Figure 5a.

Comparing the results for subcritical and critical cases presented in Figures 5 and 4, respectively, one can conclude how increasing the Reynolds number has caused the wake region to get narrower.

Approaching the higher freestream Reynolds number causes the separation bubble to shrink until it bursts. In this case, transition from laminar to turbulent occurs within the attached boundary layer. The final results at a Reynolds number of 1040000, which are presented in Figures 6a and b, go well with

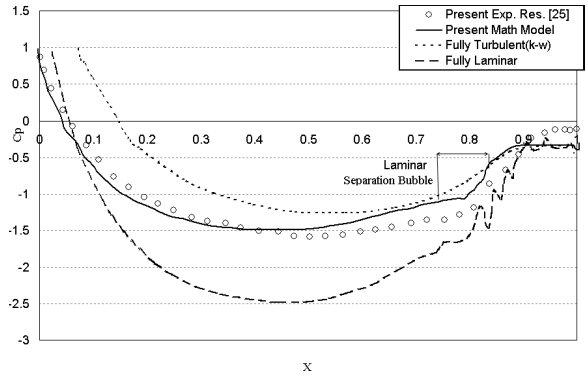

(a) Surface pressure distribution.

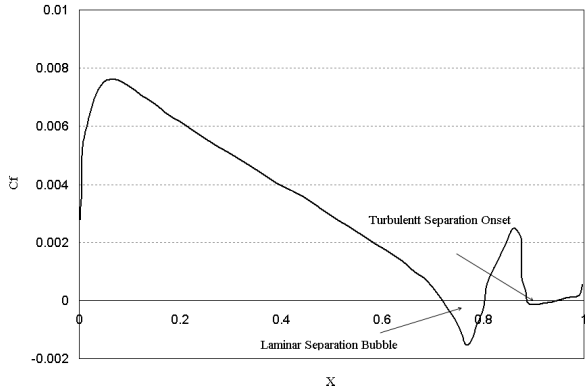

(b) Skin friction distribution.

Figure 4. Critical flow results, Re= 600000.

the above situation. As is evident from Figure 6b, transition onset has occurred around a 54% arc. This has been identified by sudden increase in the skin friction from its minimum value. Since the boundary layer is in the turbulent regime, it has resisted the adverse pressure gradient more and has remained attached to the surface for a relatively long distance downstream. No great difference in the wake size can be observed for the critical and supercritical cases (see Figures 5 and 6).

Comparison of the present numerical results with the experimental data shows very close agreement. Once again, neither the fully laminar nor the fully turbulent modeling has proved suitable for simulation of the whole flow field.

CONCLUSIONS

Occurrence of laminar separation bubbles on solid walls of an elliptic cylinder has been simulated using a recently developed transitional model for boundary layer flows. This model includes three transport equations of turbulent kinetic energy, K_T, laminar kinetic energy, K_L, and dissipation rate frequency, ω. The main conclusions withdrawn from the present research work can be categorized as follows.

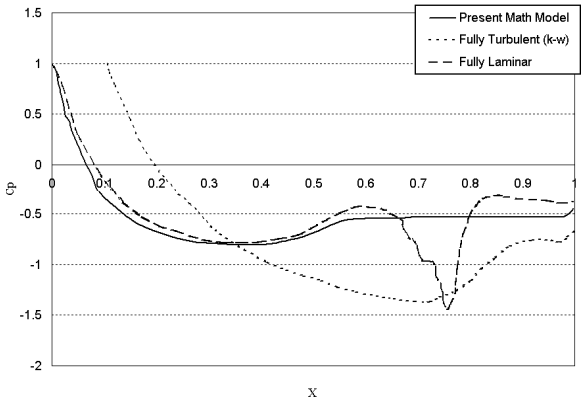

(a) Surface pressure distribution.

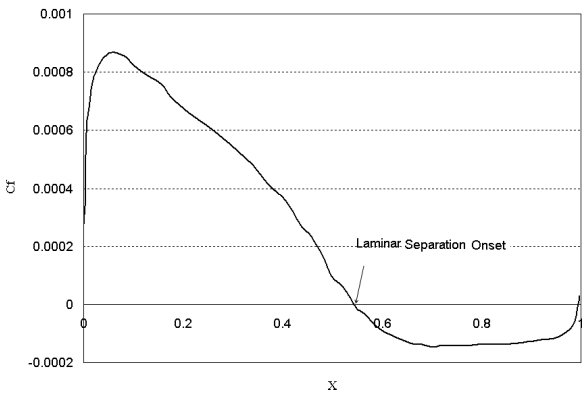

(b) Skin friction distribution.

Figure 5. Subcritical flow results, Re= 100000.

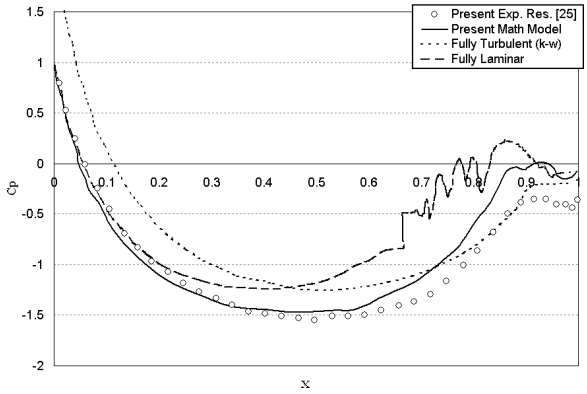

(a) Surface pressure distribution.

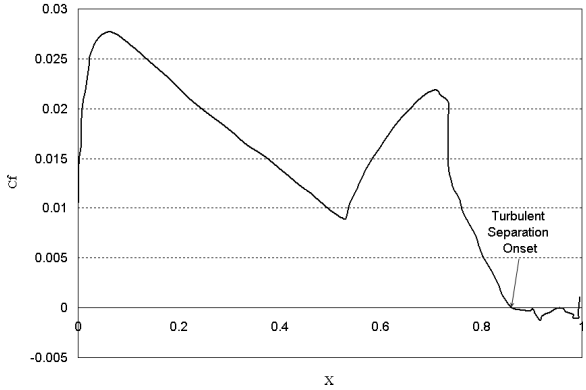

(b) Skin friction distribution.

Figure 6. Supercritical flow results, Re= 10400000.

1. The present computational model is capable of predicting laminar separation bubble, precisely.
2. The present model can be easily implemented into existing in-house or commercial CFD codes.
3. In addition to the critical flow case, the present model is capable of predicting each of the subcritical and supercritical flow regimes.

REFERENCES

1. Modi V.J., Wiland E. and Dikshit A.K., "On the Fluid Dynamics of Elliptic Cylinders", *Proceedings of the 2nd International Offshore and Polar Engineering conference*, San Francisco, USA, (1992).
2. Brandon J.M. and Ngugen L.T., "Experimental Study of Effects of Forebody Geometry on High Angle of Attack Stability", *Journal of Aircraft*, **25(7)**, PP 591-597(1988).
3. James W.D., Paris S.W. and Malcolm G.N., "Study of Viscous Cross-Flow Effects on Circular Cylinders at High Reynolds Numbers", *AIAA Journal*, **18**, PP 1066-1072(1980).
4. Holloway D., Walters K. and Leylek H., "Prediction of Unsteady, Separated Boundary Layer Over a Blunt Body for Laminar, Turbulent, and Transitional Flow", *International Journal for Numerical Methods in Fluids*, PP 1291-1315(2004).

5. Breuer M. A., "Challenging Test Case for Large Eddy Simulation: High Reynolds Number Circular Cylinder Flow", *International Journal of Heat and Fluid Flow*, **21**, PP 648-654(2000).
6. Cantwell B., Coles D., "An Experimental Study on Entrainment and Transport in the Turbulent near Wake of a Circular Cylinder", *Journal of Fluid Mechanics*, **136**, PP 321-374(1983).
7. Selvam R.P., "Finite Element Modeling of Flow Around a Circular Cylinder Using LES", *Journal of Wind Engineering and Industrial Aerodynamics*, **67-68**, PP 129-139(1997).
8. Tamura T., Ohta I., Kuwahara K., "On the Reliability of Two-Dimensional Simulation for Unsteady Flows Around a Cylinder-Type Structure", *Journal of Wind Engineering and Industrial Aerodynamics*, **35**, PP 275-298(1990).
9. Catalano P., Wang M., Iaccarino G., Moin P., "Numerical Simulation of the Flow Around a Circular Cylinder at High Reynolds Numbers", *International Journal of Heat and Fluid Flow*, **24**, PP 463-469(2003).
10. Celik I, Shaer F.D., "Long Time-Averaged Solutions of Turbulent Flow Past a Circular Cylinder", *Journal of Wind Engineering and Industrial Aerodynamics*, **56**, PP 185-212(1995).
11. Travin A., Shur M., Strelets M., Spalart P., "Detach-Eddy Simulations Past a Circular Cylinder", *Flow, Turbulence and Combustion*, **63**, PP 293-313(2000).
12. Saghaan M., Stansby P.K., Saidi M.S., Apsley D.D., "Simulation of Turbulent Flows Around a Circular Cylinder using Nonlinear Eddy-Viscosity Modeling: Steady and Oscillatory Ambient Flows", *Journal of Fluids and Structures*, **17**(8), PP 1213-1236(2003).
13. Craft T.J., Launder B.E., Suga K., "Development and Application of a Cubic Eddy-Viscosity Model of Turbulence", *International Journal of Heat and Fluid Flow*, **17**(2), PP 108-115(1996).
14. Edwards J.R., Roy C.J., Blottner F.G., Hassan H.A., "Development of a one-Equation Transition to Turbulence Model", *AIAA Journal*, **39**(9), PP 1691-1698(2001).
15. Spalart P.R., Allmaras S.R., "A one-Equation Turbulence Model for Aerodynamics Flow", *AIAA Paper, No. 92-0439*, (1992).
16. Warren ES, Hassan HA., "Transition Closure Model for Predicting Transition Onset", *Journal of Aircraft*, **35**(5), PP 769-775(1998).
17. Warren E.S., Hassan H.A., "An Alternative to the en Method for Determining the Onset of Transition", *AIAA Paper No. 97-0825*, (1997).
18. Matsubara M. and Alfredsson P.H., "Disturbance Growth in Boundary Layers Subjected to Free-Stream Turbulence", *Journal of Fluid Mechanics*, **430**, PP 149-168(2001).
19. Klebanoff P.S., "Effects of Free-Stream Turbulence on a Laminar Boundary Layer", *Bull. Am. Phys. Soc.*, **16**, (1971).
20. Mayle R.E. and Schulz A., "The Path to Predicting Bypass Transition.", *ASME Journal of Turbomachinery*, **119**, PP 405-411(1997).
21. Volino R.J., "A New Model for Free-Stream Turbulence Effects on Boundary Layers", *ASME Journal of Turbomachinery*, **120**, PP 613-620(1998).
22. 22- Bradshaw P., "Turbulence: The Chief Outstanding Difficulty of our Subject", *Experiments in Fluids*, **16**, PP 203-216(1994).
23. Jacobs R.G. and Durbin P.A., "Simulations of Bypass Transition", *Journal of Fluid Mechanics*, **428**, PP 185-212(2001).
24. Walters D.K. and Leylek J.H., "A New Model for Boundary Layer Transition Using a Single-Point RANS Approach", *ASME Journal of Turbomachinery*, **126**, PP 193-202(2004).
25. Taghavi-Zenouz R., "Aerodynamics of Bodies with Elliptical Cross-Section", Ph.D. Thesis, Aerospace Division, School of Engineering, University of Manchester, UK, (1998).